Department
of
APPLIED MATHEMATICS

Combined effects of thermohaline and atmosphere forcing on the currents at Ormen Lange

by

Øyvind Thiem[1], Tor Eldevik[1] and Jarle Berntsen[2]

Report no. 165 December 2001

UNIVERSITY OF BERGEN
Bergen, Norway

Department of Mathematics
University of Bergen
5008 Bergen
Norway

ISSN 0084-778X

Combined effects of thermohaline and atmosphere forcing on the currents at Ormen Lange

by

Øyvind Thiem[1], Tor Eldevik[1] and Jarle Berntsen[2]

[2]*Nansen Environmental and Remote Sensing Center, Bergen, Norway*
[1]*Mathematical Institute, University of Bergen.*

Report no. 165

December 2001

Combined effects of thermohaline and atmosphere forcing on the currents at Ormen Lange

Øyvind Thiem
Tor Eldevik
Nansen Environmental and Remote Sensing Center, Bergen, Norway

Jarle Berntsen
Department of Mathematics, University of Bergen, Norway

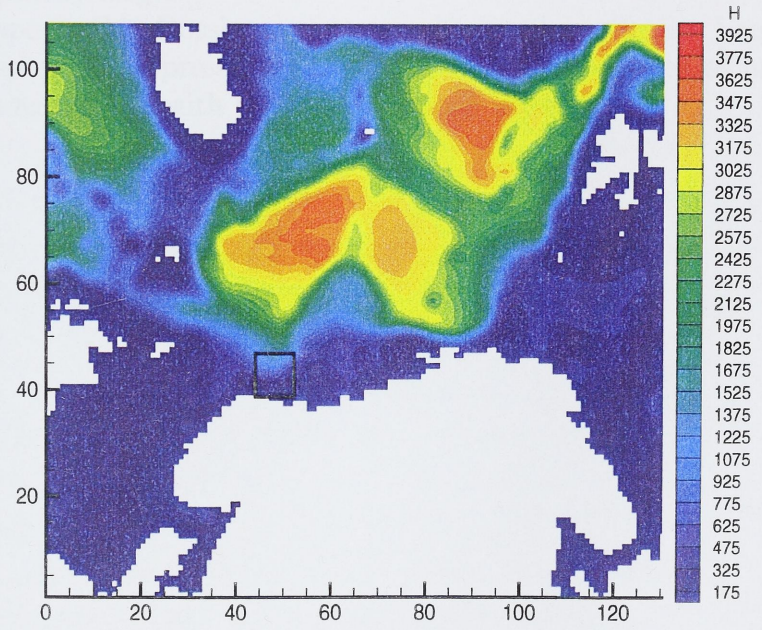

Abstract

The second largest gas field in Norway, Ormen Lange, is located at Storegga 140 km west of Kristiansund. Ormen Lange lies in the continental shelf slope where several slides have created a rough bottom topography. The depth varies between 800 to 1100 m.

A three-dimensional, time split, σ-coordinate model is used to study the combined effects of thermohaline and atmospheric forcing on the currents at Ormen Lange. Earlier studies of effects of atmospheric forcing have been performed with climatological values of temperature and salinity. Climatological fields of hydrography are generally smooth. The internal pressure forcing has therefore been too weak in previous work.

To create more realistic gradients in the density field the model has been run in 165 days and temperature and salinity fields from this experiment are used as initial and boundary values in the present study. The stronger thermohaline forcing creates a stronger thermohaline circulation, and also during strong storm events the maximum velocities at Ormen Lange may be significantly larger.

Topographic Rossby waves are generated at Ormen Lange due to the atmospheric low pressure. Periods found in time series of model velocities are in agreement with the theory of such waves.

1 Introduction

An ongoing data acquisition program at Ormen Lange, an offshore gas field located in the Storegga region off mid-Norway, has identified several events in which the currents close to the sea bed exhibit peak values in their speed and temperature over a short period of time. This may cause problems for near sea bed installations needed for exploration of the gas field. It is therefore important to understand the generation mechanisms of these events and to investigate the possibility of forecasting them.

Earlier reports (e.g., Eliassen et al. 2000) have commented on these events and suggested two plausible explanations for the high current speeds occurring at Ormen Lange. Internal waves that break towards the shelf slope or currents at strong internal density fronts. Both these explanations indicate the connection between very local strong effects and larger scale internal wave phenomena. The most pronounced generation mechanism behind internal wave phenomena in this area is atmospheric forcing, Vikebø et al. (2001).

In Vikebø et al. (2001) the generation of currents in the different water levels at the shelf and the shelf slope was investigated closer. By changing the radius, magnitude and path of an idealized atmospheric low pressure forcing the ocean surface, different scenarios where simulated.

In the present paper the additional effects of the thermohaline forcing will be investigated. Four of the events from Vikebø et al. (2001) will be simulated with corresponding boundary conditions. In Vikebø et al. (2001) the initial conditions were taken from climatological values (Engedahl et al. 1998) that are known to be too smooth spatially. The initial conditions in this paper will be taken from Eldevik et al. (2001). These initial conditions correspond to several months (165 days to be exact) spin up from the climatological data of Engedahl et al. (1998), producing relative strong thermohaline fronts.

Figures of the current speed at 10 and 50 meters above the sea bed will be made at 5 different locations in the Ormen Lange area. See Figure 1 and Figure 2. The depth at the locations are given in Table 1.

Location	OL1	OL2	OL3	OL4	OL5
Depth	257.0	499.0	835.9	1120.1	764.4

Table 1: Depths in meters at stations OL1 to OL5

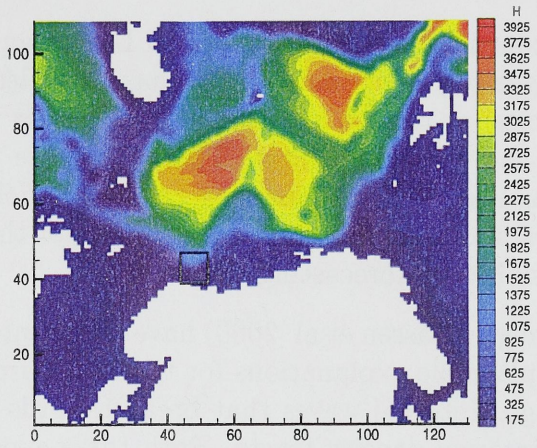

Figure 1: Model area given in grid coordinates. The grid size is 20 km. The Ormen Lange area is outlined.

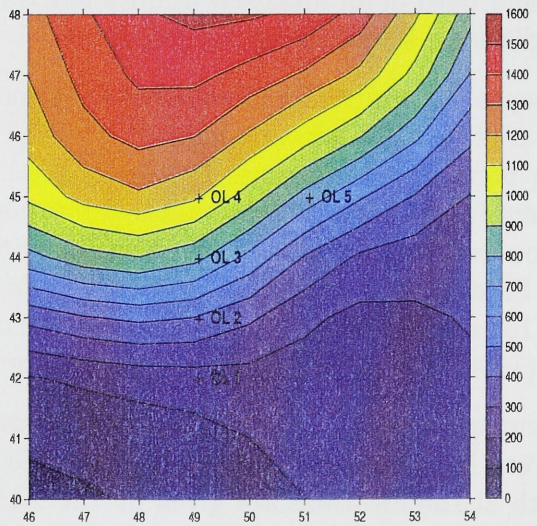

Figure 2: Ormen Lange with the locations OL1-OL5.

2 Model

This model study uses the numerical σ-coordinate ocean model of Berntsen (2000). The equations are the continuity equation for an incompressible fluid, the Reynold averaged hydrostatic momentum equations, conservation equations for temperature and salinity and the UNESCO-equation of state. The reader is referred to Berntsen (2000) for further details concerning the governing equations and numerical methods.

The model area covers the Norwegian Sea basin, see Figure 1. The horizontal grid size is 20 km. In the vertical 30 σ-layers are applied and these are distributed according to a formula given in Lynch et al. (1995). Their formula distribute the layers symmetrically about the midpoint in the vertical with a gradually finer resolution towards the surface and the bottom.

The model is run for 240 hours with an internal 3-D time step of 360 s. There are 30 2-D time steps per 3-D step. Initial values of water elevation, velocities, temperature and salinity are taken from Eldevik et al. (2001). At the lateral open boundaries, except at the boundary to the Baltic, a flow relaxation scheme (FRS) is implemented (Martinsen and Engedahl, 1987). The FRS-zones are 7 grid-cells wide. In addition to the initial values for water elevation (η), velocity (u and v), temperature (T) and salinity (S) four tidal constituents (M_2, S_2, K_1, N_2), are used to specify the lateral boundary conditions.

The flow to and from the Baltic is implemented after an algorithm due to Stigebrandt (1980). Fresh water runoff from 27 rivers around the North Sea is included. For experiments over longer periods this forcing will affect strongly the coastal circulation, but in the present study this forcing has minor importance.

Traveling low pressure systems are important driving mechanisms for the oceanic flow. Martinsen et al. (1979) constructed a model of a cyclone and studied barotropic effects of the moving cyclone. The atmospheric pressure disturbance is described by, following Martinsen et al. (1979),

$$p(x, y, t) = p_0(t) e^{\{-[(x-x_0-u_0 t)^2+(y-y_0-v_0 t)^2]/R^2\}} \quad , \tag{1}$$

where $p_0(t)$ is the pressure disturbance at the center of the cyclone, x_0, y_0 the initial position of the center of the pressure disturbance, u_0, v_0 are the x and y components of the propagation velocity and R defines the horizontal extent of the pressure disturbance. Wind velocity components u_g and v_g in x and y directions, respectively, are computed from the gradients in the atmospheric

pressure.

$$u_g = -\frac{0.7}{f\rho_a}\frac{\partial p}{\partial y} \quad , \tag{2}$$

$$v_g = \frac{0.7}{f\rho_a}\frac{\partial p}{\partial x} \quad . \tag{3}$$

Above f is the Coriolis parameter and ρ_a the density of the air ($1.3\,\mathrm{kgm}^{-3}$).

From the wind velocity, wind stress is computed

$$\tau_x = \rho_a c_D (u_g^2 + v_g^2)^{1/2} u_g \quad , \tag{4}$$

$$\tau_y = \rho_a c_D (u_g^2 + v_g^2)^{1/2} v_g \quad , \tag{5}$$

where c_D is the drag coefficient. In our experiments c_D is chosen to be 3×10^{-3} (cf. Martinsen et al. 1979).

A finding of Vikebø et al. (2001) is that the strongest response of the currents at Ormen Lange occurs when the maximum wind speed was approximately along the shelf slope. In the present study the model system will be run for the four different scenarios of Table 2. In all the experiments maximum wind speed will be approximately along the shelf slope. The model is first run for 24 hours with $p_0(t) = 0$. The low pressures are then started at positions (x_0, y_0), given in grid coordinates, see Table 2. The pressure disturbance $p_0(t)$ is increased linearly over the next 12 hours to the values given in the table and held constant for the remaining simulation periods. The propagation velocities are $u_0 = 8.59\,\mathrm{ms}^{-1}$ and $v_0 = -4.81\,\mathrm{ms}^{-1}$ in all experiments.

In the experiments with $R = 1000\,\mathrm{km}$ the shortest distance between the center of the low pressures and Ormen Lange is 667 km. The distance between the center to the point with maximum wind speed is 707 km ($R/\sqrt{2}$). When R is 500 km, the pathway of the storm is also based on the pathway given for $R = 1000\,\mathrm{km}$. The starting points (x_0, y_0) are, however, adjusted such that

Experiment		p_0	x_0	y_0	R
RUN1	(RUN_TRACK1)	-60	-12.50	115.84	1000
RUN2	(RUN_P1000)	-10	-12.50	115.84	1000
RUN3	(RUN_P10000)	-100	-12.50	115.84	1000
RUN4	(RUN_R500)	-60	-21.13	100.42	500

Table 2: Experiments discussed in this paper. In parantheses the corresponding simulations in Vikebø et al. (2001). The pressure p_0 are given in hPa and the radius R in km.

the position of maximum wind speed along the shelf slope at Ormen Lange is unchanged.

3 Model results

This section is divided into subsections for each experiment. For each experiment a table is presented with maximum speeds. The word "*Climatol*" refers to simulations run with initial conditions as discribed in Vikebø et al. (2001), and "*Spun up*" to simulations with initial conditions from Eldevik et al. (2001) as described in section 1. Time series of horizontal speed are shown in order to visualize the thermohaline effect.

The first two days are a transient phase and data from these two days are excluded from the tables.

3.1 RUN1

The low pressure at the cyclone center is p_0 = -60 hPa and the cyclone radius R = 1000 km.

10 m	*Climatol*	*Spun up*
OL1	0.380 (73.5)	0.368 (73.5)
OL2	0.305 (76.5)	0.337 (75.0)
OL3	0.141 (86.5)	0.184 (75.0)
OL4	0.094 (73.5)	0.104 (189.0)
OL5	0.157 (88.0)	0.185 (87.0)
50 m	*Climatol*	*Spun up*
OL1	0.480 (71.0)	0.459 (68.5)
OL2	0.389 (76.5)	0.422 (76.0)
OL3	0.173 (77.0)	0.239 (76.0)
OL4	0.094 (87.0)	0.124 (189.5)
OL5	0.202 (89.0)	0.243 (88.5)

Table 3: Maximum velocity in ms^{-1} at OL1-OL5, 10 and 50 m above the sea bed during low pressure passage. Times of maximum velocity occurrences in hours after simulation start are given in parenthesis.

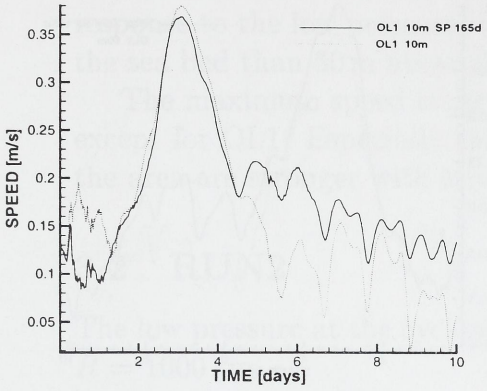

(a) OL1

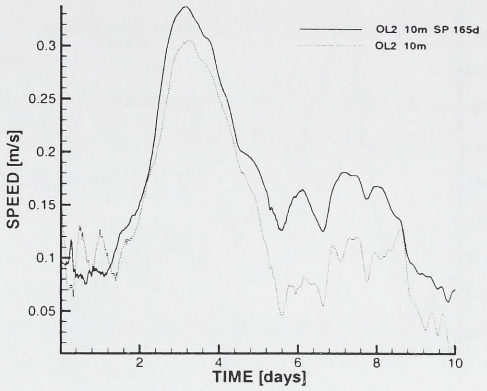

(b) OL2

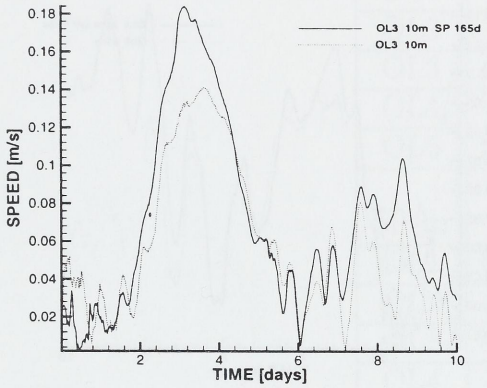

(c) OL3

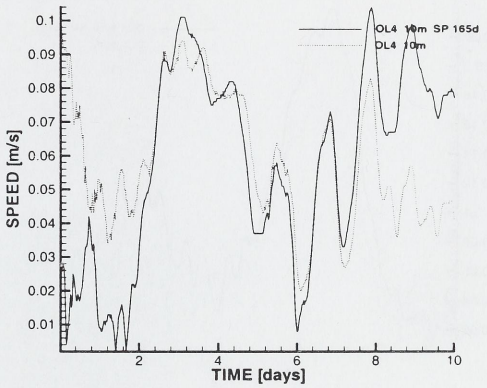

(d) OL4

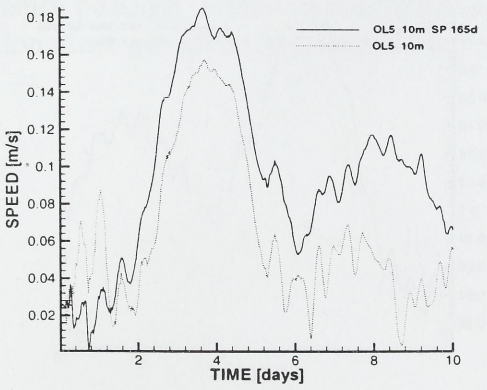

(e) OL5

Figure 3: Time series of speed OL1-OL5, 10 m above the sea bed. Solid line *Spun up* and dotted line *Climatol.*

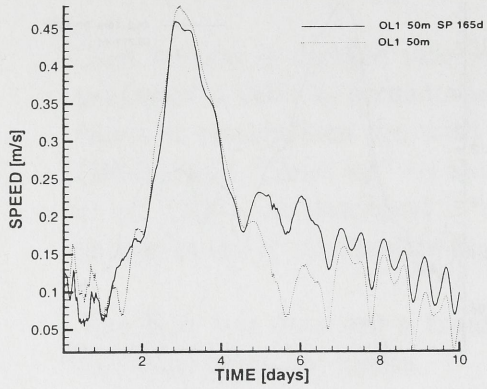

(a) OL1

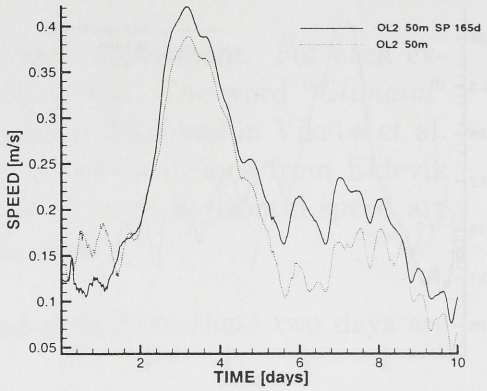

(b) OL2

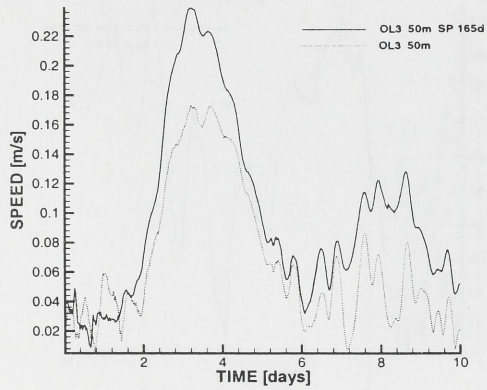

(c) OL3

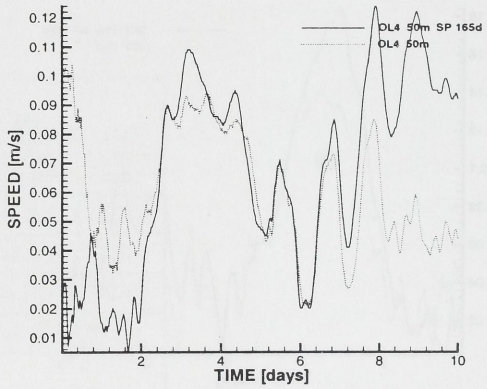

(d) OL4

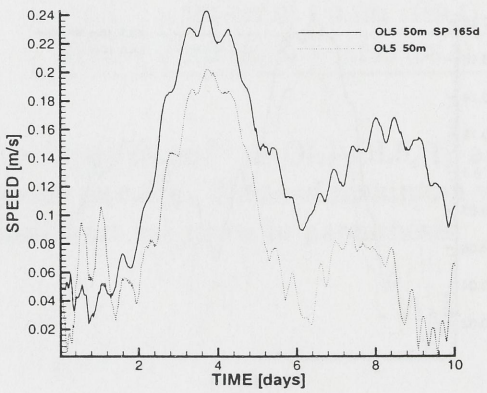

(e) OL5

Figure 4: Time series of speed OL1-OL5, 50 m above the sea bed. Solid line *Spun up* and dotted line *Climatol.*

The currents 10 m and 50 m above the sea bed show much of the same response to the low pressure. The currents are less in magnitude 10 m above the sea bed than 50 m above the sea bed, due to friction.

The maximum speed is produced by the model with spun up initial data except for OL1. Especially the currents after the storm has passed through the area are stronger with stronger density gradients.

3.2 RUN2

The low pressure at the cyclone center is p_0 = -10 hPa and the cyclone radius R = 1000 km.

10 m	*Climatol*	*Spun up*
OL1	0.153 (38.8)	0.164 (144.5)
OL2	0.119 (74.5)	0.168 (146.5)
OL3	0.042 (158.0)	0.089 (207.5)
OL4	0.053 (36.5)	0.064 (237.0)
OL5	0.051 (239.0)	0.108 (233.0)
50 m	*Climatol*	*Spun up*
OL1	0.166 (219.5)	0.184 (145.0)
OL2	0.168 (103.0)	0.207 (144.5)
OL3	0.057 (158.0)	0.121 (207.5)
OL4	0.051 (37.5)	0.075 (233.0)
OL5	0.065 (166.5)	0.150 (207.5)

Table 4: Maximum velocity in ms^{-1} at OL1-OL5, 10 and 50 m above the sea bed during low pressure passage. Times of maximum velocity occurrences in hours after simulation start are given in parenthesis.

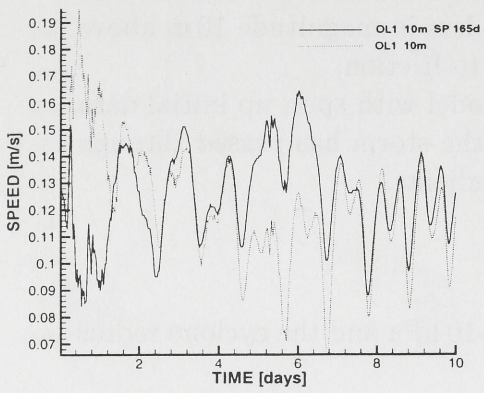

(a) OL1

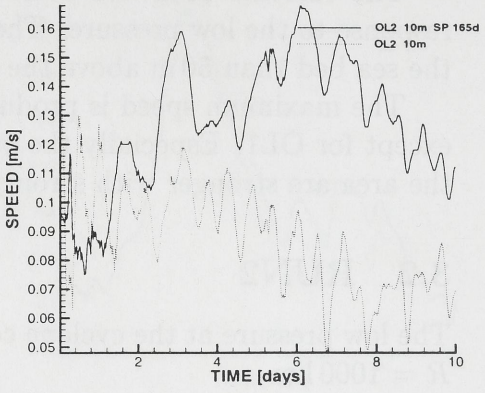

(b) OL2

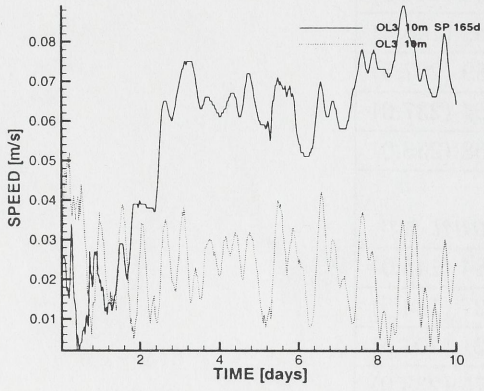

(c) OL3

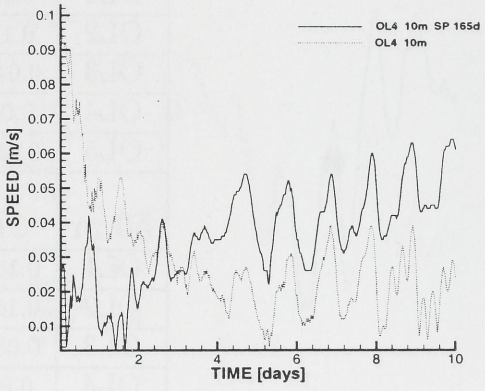

(d) OL4

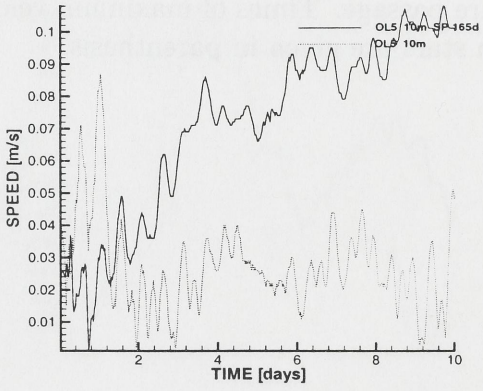

(e) OL5

Figure 5: Time series of speed OL1-OL5, 10 m above the sea bed. Solid line *Spun up* and dotted line *Climatol.*

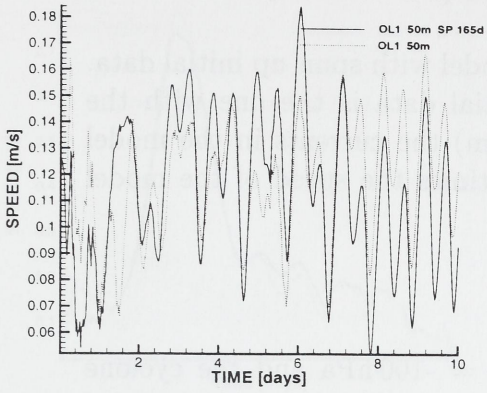

(a) OL1

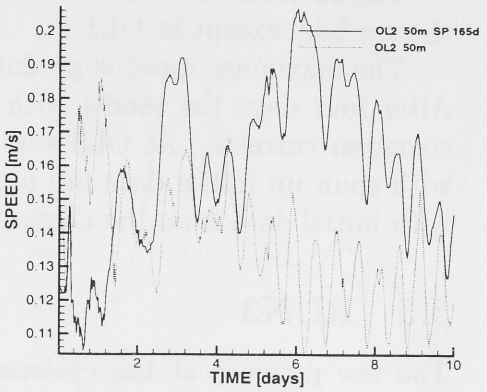

(b) OL2

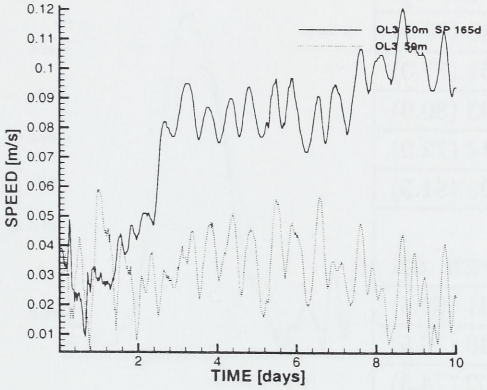

(c) OL3

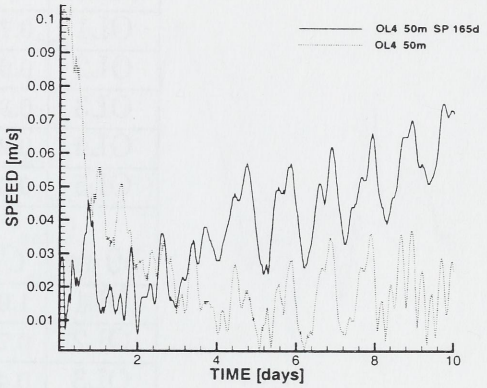

(d) OL4

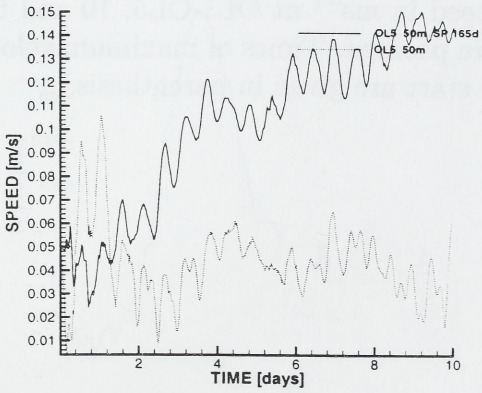

(e) OL5

Figure 6: Time series of speed OL1-OL5 50 m above sea the bed. Solid line *Spun up* and dotted line *Climatol.*

The currents show similar response to the low pressure 10 and 50 m above the sea bed, except at OL1.

The maximum speed is produced by the model with spun up initial data. After four days the model with spun up initial data is the one with the strongest currents. At OL3 and OL5 ($\sim$ 800 m) the currents in the model with spun up initial data are more than two times the speed of the model with initial data from the climatology.

3.3 RUN3

The low pressure at the cyclone center is p_0 = -100 hPa and the cyclone radius R = 1000 km.

10 m	*Climatol*	*Spun up*
OL1	0.789 (71.0)	0.740 (70.0)
OL2	0.603 (74.5)	0.651 (77.0)
OL3	0.334 (83.5)	0.393 (80.0)
OL4	0.223 (84.5)	0.214 (72.0)
OL5	0.341 (82.0)	0.393 (81.5)
50 m	*Climatol*	*Spun up*
OL1	1.004 (71.0)	0.941 (69.5)
OL2	0.777 (76.5)	0.830 (76.5)
OL3	0.420 (82.5)	0.502 (74.5)
OL4	0.264 (84.5)	0.259 (73.0)
OL5	0.431 (81.0)	0.500 (80.5)

Table 5: Maximum speed in ms^{-1} at OL1-OL5, 10 and 50 m above the sea bed during low pressure passage. Times of maximum velocity occurrences in hours after simulation start are given in parenthesis.

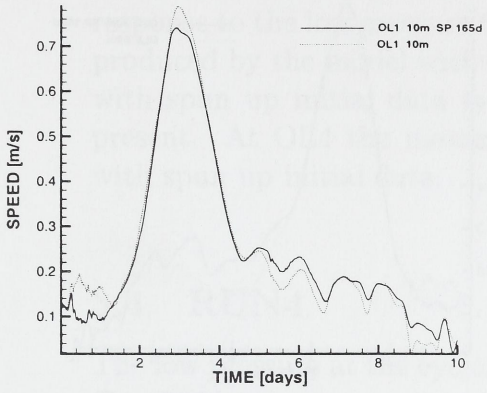

(a) OL1

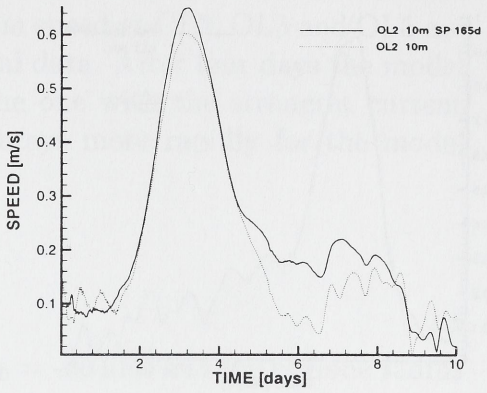

(b) OL2

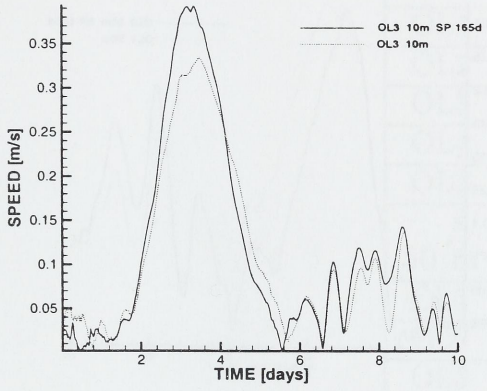

(c) OL3

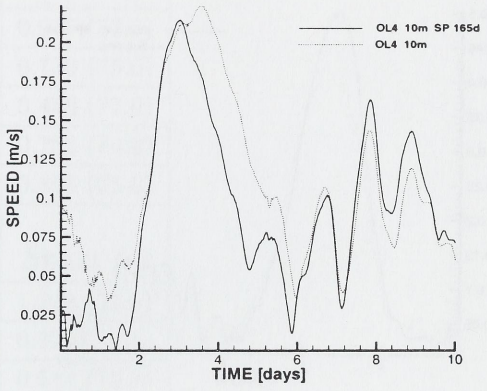

(d) OL4

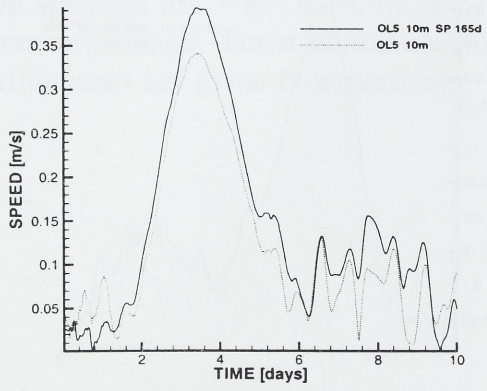

(e) OL5

Figure 7: Time series of speed OL1-OL5, 10 m above the sea bed. Solid line *Spun up* and dotted line *Climatol.*

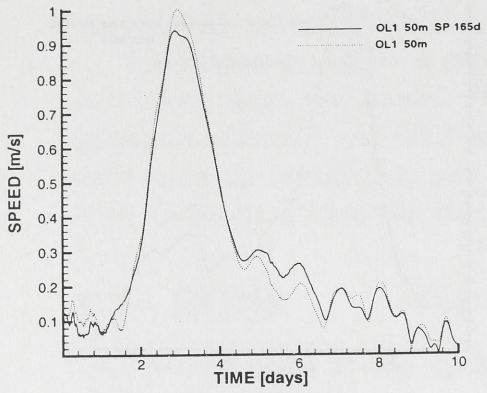

(a) OL1

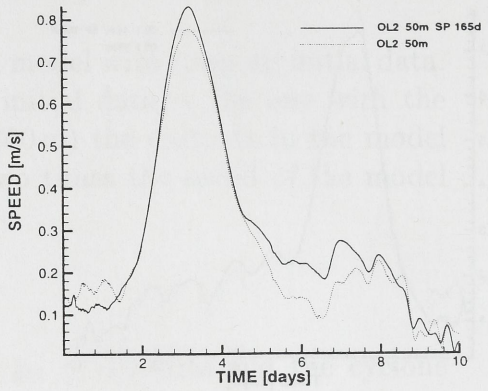

(b) OL2

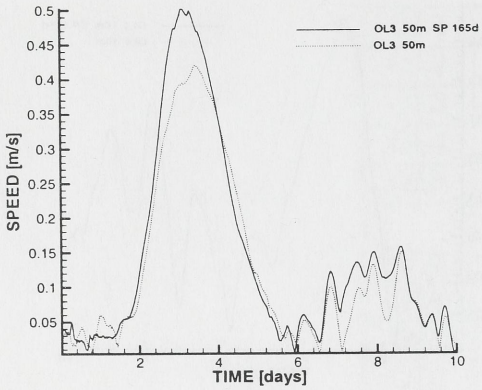

(c) OL3

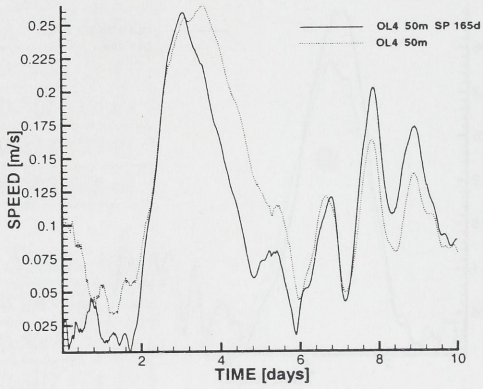

(d) OL4

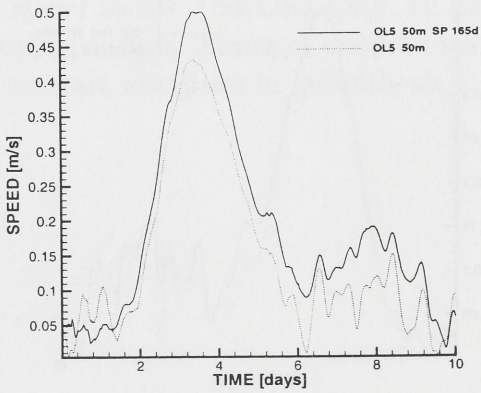

(e) OL5

Figure 8: Time series of speed OL1-OL5 50 m above the sea bed. Solid line *Spun up* and dotted line *Climatol.*

The currents 10 m and 50 m above the sea bed show much of the same response to the low pressure. The maximum speed at OL2, OL3 and OL5 are produced by the model with spun up initial data. After four days the model with spun up initial data is in general the one with the strongest current present. At OL4 the maximum speed decays more rapidly for the model with spun up initial data.

3.4 RUN4

The low pressure at the cyclone center is p_0 = -60 hPa and the cyclone radius R = 500 km.

10 m	*Climatol*	*Spun up*
OL1	0.987 (73.5)	0.947 (73.5)
OL2	0.684 (74.0)	0.730 (75.0)
OL3	0.377 (76.0)	0.453 (77.0)
OL4	0.277 (74.5)	0.292 (74.0)
OL5	0.354 (75.0)	0.398 (75.0)
50 m	*Climatol*	*Spun up*
OL1	1.269 (73.5)	1.214 (73.5)
OL2	0.885 (74.0)	0.928 (74.5)
OL3	0.492 (75.0)	0.614 (75.5)
OL4	0.330 (74.5)	0.351 (75.5)
OL5	0.436 (76.0)	0.501 (74.5)

Table 6: Maximum speed in ms^{-1} at OL1-OL5, 10 and 50 m above the sea bed during low pressure passage. Times of maximum velocity occurrences in hours after simulation start are given in parenthesis.

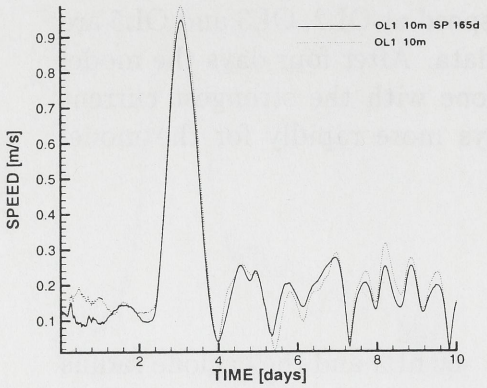

(a) OL1

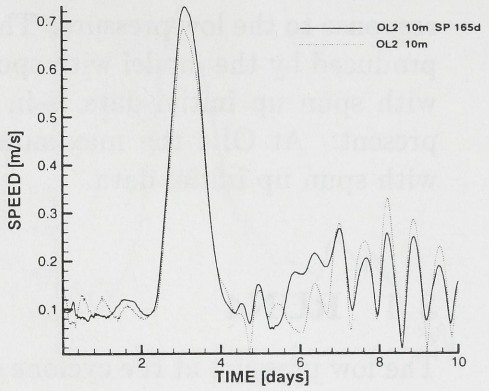

(b) OL2

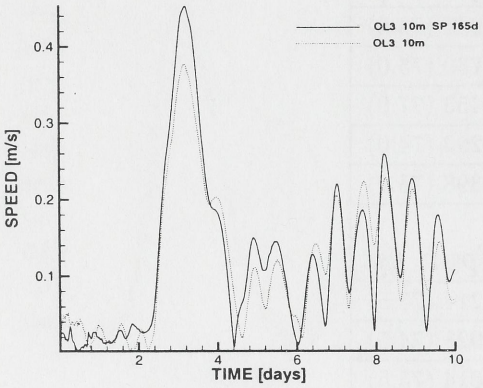

(c) OL3

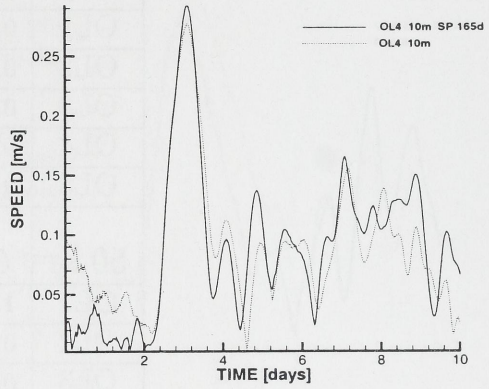

(d) OL4

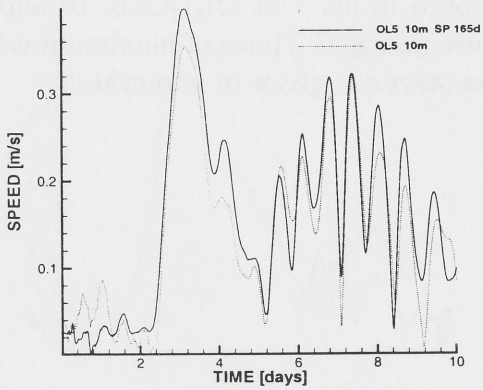

(e) OL5

Figure 9: Time series of speed OL1-OL5, 10 m above the sea bed. Solid line *Spun up* and dotted line *Climatol.*

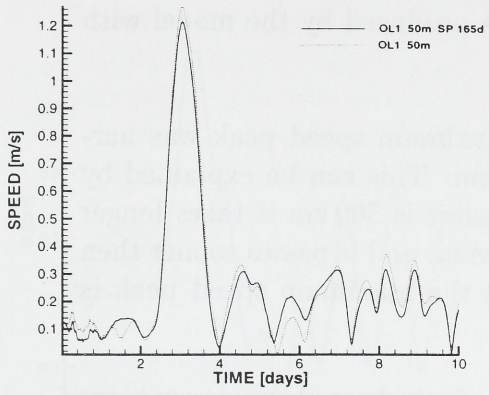

(a) OL1

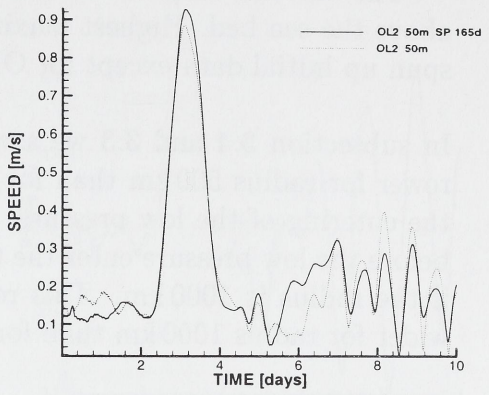

(b) OL2

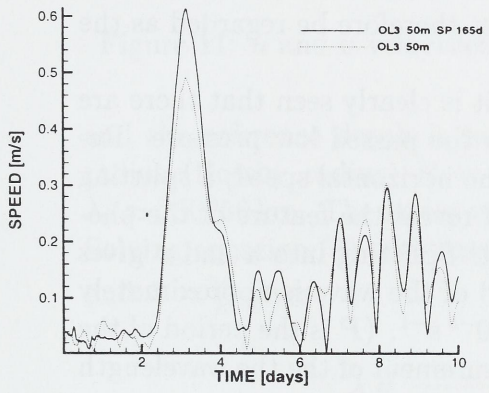

(c) OL3

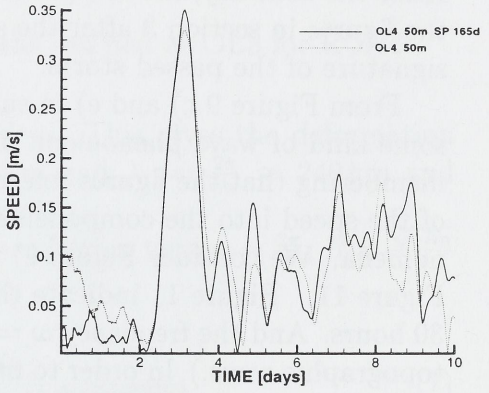

(d) OL4

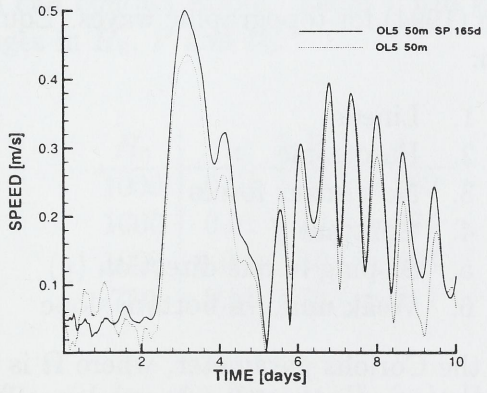

(e) OL5

Figure 10: Time series of speed OL1-OL5, 50 m above the sea bed. Solid line *Spun up* and dotted line *Climatol.*

The currents response to the low pressure is very similar 10 m and 50 m above the sea bed. Highest maximum speed is produced by the model with spun up initial data except for OL1.

In subsection 3.4 and 3.3 we saw that the maximum speed peak was narrower for radius 500 km than for radius 1000 km. This can be explained by the entering of the low pressure. When the radius is 500 km it takes longer before the low pressure enter the OL1-OL5 section, and it passes sooner then if the radius is 1000 km. This results in that the maximum speed peak is wider for radius 1000 km than for 500 km.

4 Topographic waves at Ormen Lange

From the second to the fifth day, the dominating force is the low pressure. After the fifth day, the low pressure has left the model area. What we see in the figures in section 3 after the sixth day must therefore be regarded as the signature of the passed storm.

From Figure 9 c) and e) in subsection 3.4 it is clearly seen that there are some kind of wave phenomena present due to the passed low pressure. Remembering that the figures referred to show the horizontal speed, a splitting of the speed into the components u and v will reveal the feature of the phenomena. We consider Figure c) in section 3.4. Splitting into u and v gives Figure 11. Figure 11 indicate that the period of the wave is approximately 30 hours. And the frequency $\omega = \frac{2\pi}{P} \approx 5.82 \cdot 10^{-5}\,\mathrm{s}^{-1}$. ($P$ is the period of the topographic wave.) In order to find some measurement of the the wavelength (λ) we use the equation (6)

$$\omega = \frac{\alpha_0 g}{f} \frac{k}{1 + k^2 R^2}, \tag{6}$$

from Cushman-Roisin (1994) for topographic waves. Equation (6) is derived under the assumption:

1. Linear
2. Barotropic
3. No viscous forces
4. Constant f
5. Sloping in one direction (y)
6. Weak uniform bottom slope

Here $f = 2\Omega \sin\varphi$ is the Coriolis parameter, where Ω is the rotation of the earth and $\varphi = 63,5°$ the latitude. The slope, $\alpha_0 = \frac{\Delta y}{\Delta x} = \frac{1400}{140000} = 0.01$

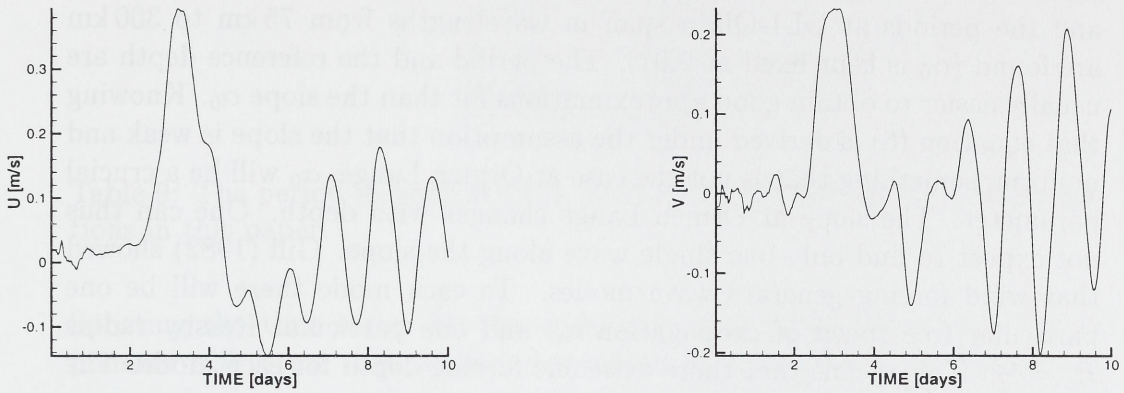

(a) u (b) v

Figure 11: u and v velocities 10 m above the sea bed at OL3 for RUN4.

and the reference depth is set to $H_0 = 850\,\text{m}$. This gives the deformation radius (Rossby radius) $R = \frac{\sqrt{gH_0}}{f} \approx 700\,\text{km}$ and $\lambda_1 = \frac{2\pi}{k} \approx 240\,\text{km}$ and $\lambda_2 \approx 260750\,\text{km}$. The latter must be excluded.
Solving equation (6) with respect on λ, remembering that $\omega = \frac{2\pi}{P}$, $R = \frac{\sqrt{gH_0}}{f}$ and $\lambda = \frac{2\pi}{k}$ gives

$$\lambda = \frac{8\pi^2 g H_0}{f(\alpha_0 g P \pm \sqrt{(P\alpha_0 g)^2 - 16\pi^2 g H_0}} \tag{7}$$

Equation (7) shows that λ depends on three parameters when we expect small changes in latitude. The reference depth H_0, the period P and the slope α_0 which all can contain errors. Table 7 will give an estimate of λ's sensitivity to changes in H_0, P and α_0.

H_0	α_0	P	λ
1000	0.01	30	≈ 282
1000	0.01	32	≈ 264
1000	0.007	30	≈ 404
750	0.01	30	≈ 211

Table 7: Sensitivity of λ (km) to H_0 (m), P (h) and α_0.

From Table 7 we see that the period and the depth do indeed alter the wavelength, but not to the same extent as the slope α_0. Using the depth and the periods at OL1-Ol5 a span in wavelengths from 75 km to 300 km are found (α_0 is kept fixed at 0.01). The period and the reference depth are usually easier to obtain good approximations for than the slope α_0. Knowing that equation (6) is derived under the assumption that the slope is weak and uniform, something that is not the case at Ormen Lange, α_0 will be a crucial parameter. The slope at Ormen Lange changes with depth. One can thus not expect to find only one single wave along the slope. Gill (1982) showed that wind forcing generate wave modes. To each mode there will be one particular free speed of propagation c_n, and one particular Rossby radius $R_n = \frac{c_n}{f}$. This means that there exist one forcing depth for each mode. The net effect seen in Figure 11 a) and b) is the superposition of all the modes present.

This wave phenomenon is found at all stations OL1-OL5. It seems to be a difference in the period depending on depth. For RUN4 the period showed an increasing tendency for increasing depth, but this was not uniform. The slope (α_0) is kept fixed. See Table 8.

Location	OL1	OL2	OL3	OL4	OL5
Depth	257.0	499.0	835.9	1120.1	764.4
Period	29.3	29.0	30.7	30.8	31.7

Table 8: Connection between period (h) and depth (m).

Solving equation (6) with respect to P gives

$$P = \frac{\lambda^2 f^2 + 4\pi^2 g H_0}{\alpha_0 g \lambda f}, \tag{8}$$

which shows that an increase in period is expected for an increase in depth. Figure 2 shows that for OL2, OL3 and OL4 the slope is almost uniform. A growth in period with depth is expected for these locations. This fits with the results from Table 8. It is also seen from equation (8) that a steep slope (growing α_0) gives decay in period. Since OL1 is located in an area that is not as steep as OL2, this can explain why OL1's period is longer then OL2's. OL5 is not located at the same straight line as OL1-OL4, see Figure 2. This means that more than the slope parameter α_0 is changed.

Experiment	P
RUN1	25.6
RUN2	25.2
RUN3	28.6
RUN4	30.7

Table 9: The period in hour at OL3, 50 m above the sea bed for the simulations in this paper.

Splitting the time series for the speed into time series for u and v components will reveal that similar phenomena also are present for the weaker storms. In these cases the speed will be less, and that means the topographic wave phenomena is expected to be more influenced by the advection of the flow. This makes it more difficult to determine a period of the topographic wave. At OL3 the period P are calculated for the different storm scenarios, see Table 9. This indicate a link between the period of a topographic shelf wave and the gradient (the forcing) of the low pressure. As Table 9 shows, a weak low pressure give shorter period than a strong low pressure. The power of a low pressure is given by the gradient of the low pressure. The gradient can be regarded as

$$G \sim \frac{p}{R}, \tag{9}$$

where G is the gradient of the low pressure, p is the pressure and R is the radius of the low pressure. This is summarized in Table 10.

Experiment	G
RUN1	-0.006
RUN2	-0.001
RUN3	-0.010
RUN4	-0.012

Table 10: The low pressure gradient in N/m^3.

From Table 10 we can see that the atmospheric forcing in RUN4 is twice as strong as for RUN1. If we compare the figures from subsection 3.1 and 3.4 we see that there is a certain agreement between the atmospheric forcing and the speed that occurs at OL1-OL5.

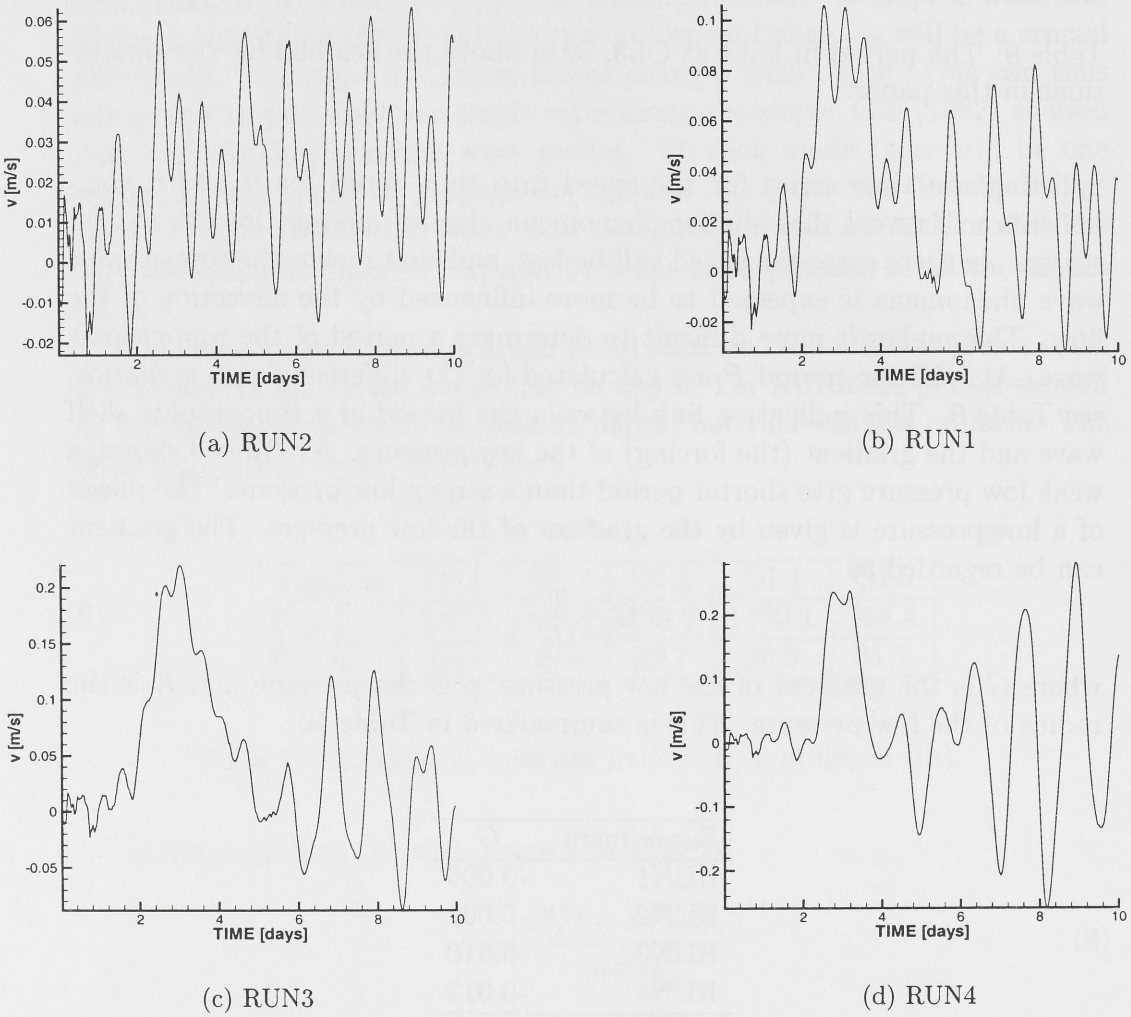

(a) RUN2

(b) RUN1

(c) RUN3

(d) RUN4

Figure 12: Velocity in y-direction (v) at OL3 50 m above the sea bed for the four scenarios in this report.

After 6 days, figure 12 a)-d) reveals that the two periods in hours (not exact)

$$P_{\frac{f}{2}} = \frac{2\pi}{\frac{f}{2}} = 26.9 \tag{10}$$

$$P_f = \frac{2\pi}{f} = 13.9 \tag{11}$$

are present. One interesting feature is that for powerful low pressure gradients as in Figure 12 d), the period $P_{\frac{f}{2}}$ in equation (10) is dominating throughout the simulation. Weaker low pressure gradients allow the period P_f in equation (11) to reveal itself earlier. Figure 12 b) and c) also show that when P_f appear this can cause dramatic fall in speed. For these two figures the maximum velocity between day 9 and 10 are reduced to half the maximum velocity between day 7 and 9.

5 Temperature versus speed

Observations from Ormen Lange, Vikebø et al. (2001), show that changes in temperature and speed often are connected. The numerical results show similar behavior for temperature and speed at Ormen Lange. Flow up or down will rise or sink the isotherms and also cause mixing between the warm Atlantic Water (upper) and the colder Norwegian Sea Arctic Intermediate Water (lower). It was found that an increase in speed usually led to an increase in temperature. The increase in speed came before the temperature change. As examples see Figure 13 (a) and (b). Notice that rapid change in speed leads to rapid change in temperature.

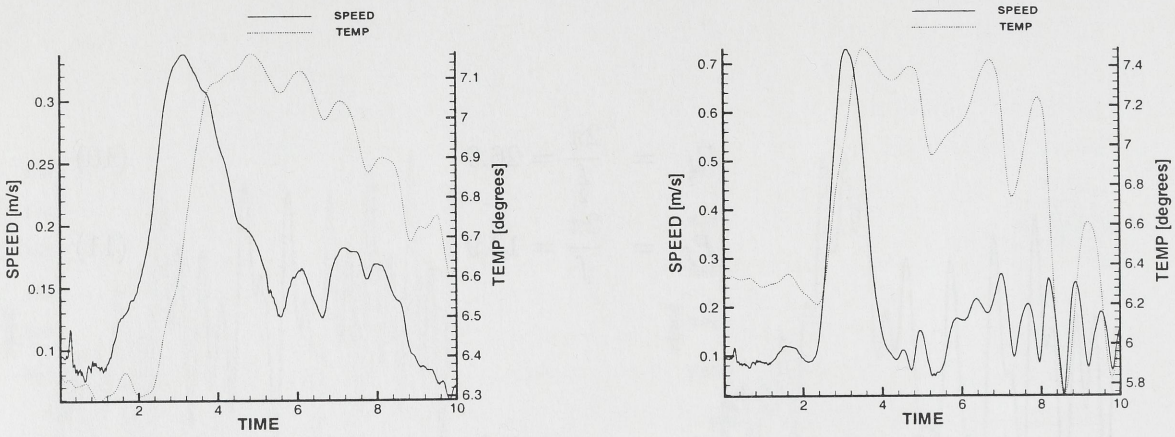

(a) RUN1 (b) RUN4

Figure 13: Increase in speed usually leads to increase in temperature. The figures are from OL2, 10 m above the sea bed.

The results also showed that strong storms as in subsections 3.3 and 3.4 led to temperature differences that was stronger and maximum currents that was higher than for weaker storms as in subsection 3.2.

6 Discussion

In the present studies a three-dimensional, time split, σ-coordinate model is used to study the combined effects of thermohaline and atmospheric forcing on the currents at Ormen Lange. Earlier studies of effects of atmospheric forcing have been performed with climatological values of temperature and salinity (Vikebø et al. 2001). Climatological fields of hydrography are generally smooth. The internal pressure forcing has therefore been too weak in previous work.

To create more realistic gradients in the density field the model has been run in 165 days (Eldevik et al. (2001)) and temperature and salinity fields from this experiment are used as initial and boundary values in the present study. The stronger thermohaline forcing creates a stronger thermohaline circulation.

The dominating force in the numerical experiments is the atmospheric forcing. The model results show that a strong thermohaline field leads to an increase in maximum speed. The relative increase is dependent on the magnitude of the storm.

In experiments with a weak low pressure the maximum speed is doubled in some locations when stronger thermohaline effects are added.

For more powerful storms the maximum increase in speed is limited to 25 percent of the speed for the model with initial conditions from climatological values at approximately 800 m depth.

For shallow sections the thermohaline effect has not the same influence on the maximum current as it has for deeper sections. This seems reasonable since density gradients at the upper shelf slope and the shelf break are small due to the dominance of the warm and salt Atlantic Water (AW).

The strongest change in temperature is at about 800 m depth when the incoming storm is powerful. The magnitude of the low pressure determines the magnitude of the temperature change. The interface between AW and the fresh and colder Norwegian Sea Arctic Intermediate Water (NSAIW) is usually located at approximately 500 m depth. When strong low pressures are present in the simulations, the interface of AW and NSAIW is shown to be dragged down the shelf slope to at least 800 m depth. This leads to the large rise in temperature at deeper stations. For weaker storms, the shallower sections has approximately the same temperature change as deeper sections.

The experiments reveal that low pressure certainly is an important generation mechanism for topographic Rossby waves (continental shelf waves) at Ormen Lange. In this paper linear theory is used in order to get a dispersion relation. It should be noted that this theory probably is too simplified for this complex system at hand. The dispersion relation is used to study which

parameters the period/wavelength depend on. The period of this wave phenomenon is a superposition of modes. We found that the period depends at least on the wavelength, the depth, the slope, the forcing and the latitude. The numerical results show that if the atmospheric pressure gradient is increased, the period of the topographic wave becomes longer. The wavelength is expected to lie in the interval 75 – 400 km.

In this study the effects that are expected to play a significant role in generating currents at Ormen Lange are discussed. The simulations also include other effects such as tidal forcing and runoff from rivers. With grid size 20 km there will be important processes that are not resolved by the model. These processes may play an important role for magnitude of the currents. Bottom topography that is expected to be a generator for such small scale phenomena is poorly resolved. To resolve more of the topography and oceanic phenomena, a first step will be to run the model system with 4 km horizontal resolution for large parts of the Norwegian Sea, including the Ormen Lange area. Results from such higher resolution studies may then be used to force even finer resolution studies focusing on Ormen Lange.

Acknowledgement

This work has been supported by Norsk Hydro though grants NHT-B44-5113464-00 and NHT-B44-5098606-00.

References

[1] J. Berntsen. USERS GUIDE for a modesplit σ-coordinate numerical ocean model. Technical Report 135, Dept. of Applied Mathematics, University of Bergen, Johs. Bruns gt.12, N-5008 Bergen, Norway, 2000. 48p.

[2] B. Cushman-Roisin. *Introduction to Geophysical Fluid Dynamics.* Prentice Hall, 1994. ISBN-0-13-353301-8.

[3] T. Eldevik, I. Eliassen, J. Berntsen, and G. Furnes. On the influence of the thermohaline circulation at Ormen Lange. Technical report, Dept. of Applied Mathematics, University of Bergen, Johs. Bruns gt.12, N-5008 Bergen, Norway, 2001. 29p.

[4] I. Eliassen, T. Eldevik, J. Berntsen, and G. Furnes. The current conditions at Ormen Lange - Storegga. Technical report, Dept. of Applied Mathematics, University of Bergen, Johs. Bruns gt.12, N-5008 Bregen, Norway, 2000. 22p.

[5] H. Engedahl, B. Ådlandsvik, and E.A. Martinsen. Production of monthly mean climatological archives of salinity, temperature, current and sea level for the Nordic Seas. *J. Mar. Syst.*, 14:1–26, 1998.

[6] A.E. Gill. *Atmosphere-Ocean Dynamics.* Academic Press, 1982. ISBN-0-12-283520-4.

[7] D.R. Lynch, J.T.C. Ip, C.E. Naimie, and F.E. Werner. Convergence studies of tidally-rectified circulation on Georges Bank. In D.R. Lynch and A.M. Davies, editors, *Quantitative Skill Assessment for Coastal Ocean Models.* American Geophysical Union, 1995.

[8] E.A. Martinsen and H. Engedahl. Implementation and testing of a lateral boundary scheme as an open boundary condition in a barotropic ocean model. *Coastal Engineering*, 11:603–627, 1987.

[9] E.A. Martinsen, B. Gjevik, and L.P. Røed. A numerical model for long barotropic waves and storm surges along the western coast of Norway. *J.Phys.Oceanogr.*, 9:1126–1138, 1979.

[10] A. Stigebrandt. Barotropic and baroclinic response of a semi-enclosed basin to barotropic forcing of the sea. In H.J. Freeland, D.M. Farmer, and C.D. Levings, editors, *Proceeding of the NATO Conference on Fjord Oceanography.* Plenum Press, New York, 1980.

[11] F. Vikebø, J. Berntsen, and G. Furnes. Analysis of events at Ormen Lange: measurements and modelling. Technical report, Dept. of Applied Mathematics, University of Bergen, Johs. Bruns gt.12, N-5008 Bergen, Norway, 2001.

[12] F. Vikebø, J. Berntsen, and G. Furnes. Numerical studies of the response of currents at Ormen Lange to travelling storms. Technical report, Dept. of Applied Mathematics, University of Bergen, Johs. Bruns gt.12, N-5008 Bergen, Norway, 2001.